BIOCHEMISTRY
including biophysical chemistry & molecular biology

Article

pubs.acs.org/biochemistry

# Thermodynamics of Coupled Folding in the Interaction of Archaeal RNase P Proteins RPP21 and RPP29

Yiren Xu,[†,‡,§,∥] Sri Vidya Oruganti,[‡,§] Venkat Gopalan,[†,‡,§] and Mark P. Foster*[,†,‡,§]

[†]Ohio State Biochemistry Program, The Ohio State University, Columbus, Ohio 43210, United States
[‡]Department of Biochemistry, The Ohio State University, Columbus, Ohio 43210, United States
[§]Center for RNA Biology, The Ohio State University, Columbus, Ohio 43210, United States

Supporting Information

**ABSTRACT:** We have used isothermal titration calorimetry (ITC) to identify and describe binding-coupled equilibria in the interaction between two protein subunits of archaeal ribonuclease P (RNase P). In all three domains of life, RNase P is a ribonucleoprotein complex that is primarily responsible for catalyzing the $Mg^{2+}$-dependent cleavage of the 5′ leader sequence of precursor tRNAs during tRNA maturation. In archaea, RNase P has been shown to be composed of one catalytic RNA and up to five proteins, four of which associate in the absence of RNA as two functional heterodimers, POP5−RPP30 and RPP21−RPP29. Nuclear magnetic resonance studies of the *Pyrococcus furiosus* RPP21 and RPP29 proteins in their free and complexed states provided evidence of significant protein folding upon binding. ITC experiments were performed over a range of temperatures, ionic strengths, and pH values, in buffers with varying ionization potentials, and with a folding-deficient RPP21 point mutant. These experiments revealed a negative heat capacity change ($\Delta C_p$), nearly twice that predicted from surface accessibility calculations, a strong salt dependence for the interaction, and proton release at neutral pH, but a small net contribution from these to the excess $\Delta C_p$. We considered potential contributions from protein folding and burial of interfacial water molecules based on structural and spectroscopic data. We conclude that binding-coupled protein folding is likely responsible for a significant portion of the excess $\Delta C_p$. These findings provide novel structural and thermodynamic insights into coupled equilibria that allow specificity in macromolecular assemblies.

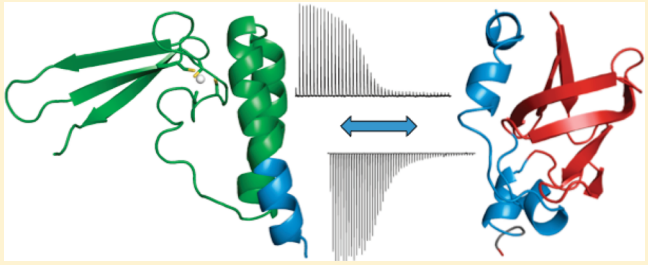

We have used isothermal titration calorimetry (ITC) to identify and describe the thermodynamics of binding-coupled equilibria in the interaction between two protein subunits of archaeal ribonuclease P (RNase P), a ribonucleoprotein (RNP) complex that is primarily responsible for endonucleolytic removal of the 5′ leader sequence during tRNA maturation.[1−3] RNase P was first shown to function as a ribozyme in bacteria, where the mass ratio of the large catalytic RNase P RNA (RPR) to the small protein [RNase P protein (RPP)] is 90:10.[4] In contrast, the RPR in eukaryotes is accompanied by nine proteins, accounting for 70% of the mass of eukaryal RNase P.[1,2,3,5] Archaeal RNase P appears to be an intermediate between bacterial and eukaryal enzymes, with four to five RPPs and an ∼50:50 RNA:protein mass ratio.[1−3] Interestingly, the increased RPP content in RNase P is associated with a decrease in the pre-tRNA cleavage catalytic activity of the isolated RPR in the three domains of life.[2,6−9] Thus, comparative studies of these RNase P variants will help address the manner by which protein cofactors might subsume some of the structural and functional responsibilities of the RNA catalyst.

Recent attention has been drawn to archaeal RNase P because of its resemblance to the eukaryal enzyme, with a simpler architecture.[10] Five distinct proteins have been identified to be associated with the RPR in *Pyrococcus furiosus* (*Pfu*) RNase P, four of which function as two binary complexes.[10,11] POP5−RPP30 has been shown to interact with the catalytic domain (C-domain) of the RPR and enhances the cleavage rate, $k_{cat}$,[12,13] while RPP21−RPP29 binds to the RPR specificity domain (S-domain) and increases substrate affinity, $K_S$.[12,14] The fifth protein, L7Ae, is thought to recognize a kink−turn (K-turn) structural motif on the RPR and has been shown to elevate the temperature of optimal activity of the enzyme reconstituted in vitro from 55 to 70 °C.[15,16]

Nuclear magnetic resonance (NMR) studies of the *Pfu* RPP21 and RPP29 proteins in isolation and in their 30 kDa 1:1 complex showed that several structural elements observed in the complex are poorly formed in the free proteins.[14,17] Structural studies of RPPs from several archea, including *Pfu* and the highly homologous *Pyrococcus horikoshii* (*Pho*), have revealed that RPP21 is a member of the zinc ribbon fold family, with an N-terminal helix−turn−helix motif,[17,18] while RPP29 is a member of the Sm fold family, consisting of a central $\beta$ barrel with helices at both N- and C-termini.[19−21] Both *Pfu* RPP21

**Received:** November 6, 2011
**Revised:** December 19, 2011
**Published:** December 22, 2011

  

and RPP29 are highly basic proteins, with isoelectric points (pI) estimated to be 10.3 and 10.2, respectively (http://web.expasy.org/protparam/), as consequence of a high proportion of positively charged Lys or Arg residues (RPP21, 30%; RPP29, 20%). The assembled RPP21−RPP29 complex projects an extensive electropositive surface on one side, possibly for complementary electrostatic pairing with the negatively charged surface of the RNA subunit.[14] Their protein−protein interface is composed of helices 1−4 and strand $\beta$2 of RPP29 and the N-terminal helices of RPP21 (Figure 1 and Figure S1 of the Supporting Information) and is characterized by both hydrophobic and electrostatic interactions, leading to a surface burial of ~2400 Å$^2$. A large fraction of the region comprising this interface, a total of 50 residues, including residues 17−48 and 116−123 of RPP29 and residues 9−18 of RPP21, is insufficiently structured in the isolated proteins to produce observable NMR signals (because of dynamic exchange between multiple conformations on time scales that lead to signal broadening) but becomes structured and can be observed by NMR in the presence of its partner.[14,17]

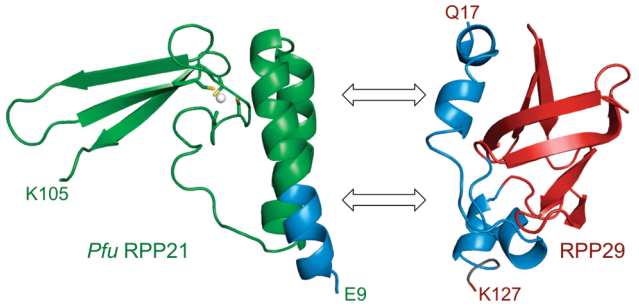


**Figure 1.** Structures of *Pfu* RPP21 and RPP29 as observed in their complex.[14,17] The proteins adopt folds commonly observed in RNA-binding proteins. RPP21 is a zinc ribbon, while RPP29 is a member of the family of Sm-like proteins. Ribbon diagrams are colored to indicate the structured cores of RPP21 (green) and RPP29 (red) based on NMR studies, with the segments that become ordered upon binding highlighted in blue. For RPP21, zinc-chelating cysteines are shown as sticks and zinc is shown as a sphere.

In this paper, we report the thermodynamic characterization of the *Pfu* RPP21−RPP29 association using isothermal titration calorimetry (ITC). The heat capacity change accompanying complex formation, $\Delta C_{p,\mathrm{obs}}$, was measured as a means of assessing the thermodynamic impact of the spectroscopically observed coupled folding during the specific interaction between the proteins.[22] A $\Delta C_{p,\mathrm{obs}}$ much more negative than that predicted from changes in solvation from the accessible surface area, ΔASA, buried in the interface between the proteins was determined (i.e., the hydrophobic effect). To assess the correlation between this thermodynamic parameter and structural insights related to the extent of coupled folding observed by NMR, we considered other thermodynamic linkages that could contribute to $\Delta C_{p,\mathrm{obs}}$ (ion, proton, and water) and uncovered important correlations to folding and binding. These insights were corroborated through analysis of a point mutant (RPP21/A14V) that exhibits less coupled folding on the basis of NMR analysis and a smaller $\Delta C_{p,\mathrm{obs}}$. This structural−thermodynamic analysis has yielded important correlations between global thermodynamic measurements and the details of residue-specific interactions that allow assembly of the RPP21−RPP29 complex. These insights may prove to be generally applicable for understanding the assembly of multisubunit RNP complexes.

## MATERIALS AND METHODS

**Structural−Thermodynamic Calculations.** The extent and character of the RPP21−RPP29 intermolecular interface were analyzed using the VADAR webserver (http://vadar.wishartlab.com/),[23] with the default parameters for definitions of radii and residue polarity and method of surface calculation. The coordinates from all 10 models of the NMR structure of the *Pfu* RPP21−RPP29 complex [Protein Data Bank (PDB) entry 2KI7] were used as input to VADAR either intact or after separating coordinates for the two chains. The mean and standard deviation of intermolecular polar and nonpolar surface burial were obtained by comparing the accessible surface areas of the complex and individual chains. A structurally predicted heat capacity change, $\Delta C_{p,\mathrm{str}}$, was computed from the change in accessible polar and nonpolar surface from the empirical relation[24]

$$\Delta C_{p,\mathrm{str}} = 0.45\Delta\mathrm{ASA}_{\mathrm{np}} - 0.26\Delta\mathrm{ASA}_{\mathrm{polar}} \quad (1)$$

where $\Delta\mathrm{ASA}_{\mathrm{np}}$ and $\Delta\mathrm{ASA}_{\mathrm{polar}}$ are the changes in surface accessible nonpolar and polar or charged surface area, respectively.

**Sample Preparation.** The *Pfu* RPP29 and RPP21 proteins were overexpressed and purified as previously described.[14,17,25] The same purification procedure that was used for wild-type RPP21 was used to obtain purified *Pfu* RPP21/A14V, in which Ala14 had been mutated to Val. After dialysis into the NMR buffer individually [10 mM Tris (pH 6.7), 10 mM KCl, 0.3 mM $ZnCl_2$, and 0.02% $NaN_3$], each protein solution (<2 mL) was transferred into membrane tubing (Spectra/Por 3 dialysis tubing, 3.5K molecular weight cutoff), and both proteins were dialyzed twice for ≥6 h in the same container against a 250−350-fold excess of standard ITC buffer [20 mM cacodylate (pH 6.7), 10 mM KCl, 0.3 mM $ZnCl_2$, and 0.02% $NaN_3$] at 22 °C. Cacodylate buffer was chosen because of its small ionization heat change from −0.41 kcal/mol at 10 °C to −1.33 kcal/mol at 55 °C, resulting in a relatively temperature-independent pH within the experimental temperature range.[26] Protein concentrations were determined from extinction coefficients calculated on the basis of their amino acid sequence (37470 $M^{-1}$ $cm^{-1}$ for *Pfu* RPP29 and 16180 $M^{-1}$ $cm^{-1}$ for *Pfu* RPP21) at 280 nm (http://www.expasy.ch/tools/protparam.html). The ITC samples were further diluted to the desired concentrations using the same batch of buffer that was used for dialysis and were thoroughly degassed under vacuum with gentle stirring before being used.

**Isothermal Titration Calorimetry.** All ITC experiments were conducted on a VP-ITC calorimeter (MicroCal, Inc., Northampton, MA) with a first 3 $\mu$L injection (discarded during analysis) followed by a series of 5 $\mu$L injections with at least 400 s between each injection. The measured heat pulses for each injection were integrated and normalized per mole of the injectant to obtain the binding enthalpy, $\Delta H_{\mathrm{obs}}$. Heats of dilution were obtained by averaging the last few integrated heat pulses after saturation, and that value was subtracted from all the integrated heat pulses. The corrected $\Delta H_{\mathrm{obs}}$ values were plotted as a function of molar ratio and fit via nonlinear least-squares regression to a single-binding site model to obtain values of stoichiometry ($N$) and association constant ($K_A$). The Gibbs free energy of binding ($\Delta G_{\mathrm{obs}}$) and entropy change

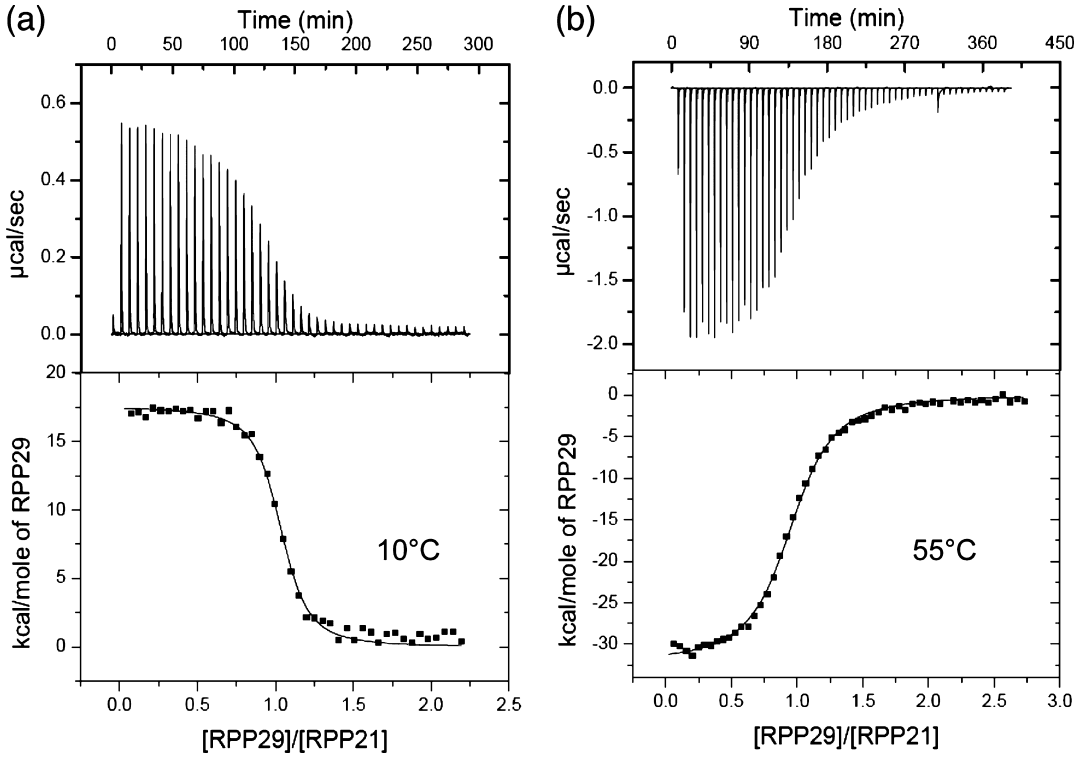


**Figure 2.** Calorimetric titration of RPP29 to RPP21 is endothermic at 10 °C (a) and exothermic at 55 °C (b) in standard ITC buffer [20 mM cacodylate (pH 6.7), 10 mM KCl, 0.3 mM $ZnCl_2$, and 0.02% $NaN_3$]. Each peak (top panels) shows the power required to maintain a fixed temperature difference with respect to the reference cell upon injection of 5 $\mu$L of 200 $\mu$M RPP29 into 20 $\mu$M RPP21. The integrated heats were normalized per mole of ligand (RPP29), corrected for the heat of dilution, and fit to a single-binding site model by nonlinear least-squares analysis (bottom panels). Best-fit values are listed in Table 1.

($\Delta S_{obs}$) were obtained from the Gibbs relation:

$$\Delta G = -RT \ln K_A = \Delta H - T\Delta S \quad (2)$$

where $R$ is the gas constant and $T$ is the temperature in kelvin.

The bulk thermodynamics of the interactions are more completely described with a measurement of the heat capacity change of binding ($\Delta C_p$), which defines the temperature dependence of $\Delta H$ and $\Delta S$:

$$\Delta H(T) = \Delta C_p(T - T_H) \quad (3)$$

$$\Delta S(T) = \Delta C_p \ln(T/T_S) \quad (4)$$

where $T_H$ and $T_S$ are the temperatures at which the net binding $\Delta H$ and $\Delta S$ values are zero, respectively. Thus, $\Delta C_p$ was obtained from the slope of $\partial\Delta H/\partial T$ in titrations of RPP29 into RPP21 performed over the temperature range of 10−55 °C.[27] $T_S$ was obtained from the modified Gibbs−Helmholtz relation, which combines eqs 2−4:

$$\Delta G(T) = \Delta C_p(T - T_H) - T\Delta C_p \ln(T/T_S) \quad (5)$$

Likewise, titrations of RPP29WT into RPP21/A14V were performed in standard ITC buffer from 5 to 55 °C, yielding $\Delta H_{obs}$, and subsequently $\Delta C_{p,obs}$.

**Ion and Proton Linkage Effect.** Protein stock solutions were thoroughly dialyzed twice in standard ITC buffer containing 50, 100, and 150 mM KCl. A reverse titration of RPP21 into RPP29 was performed because of the low solubility of RPP29 at KCl concentrations of >150 mM. The ion linkage number was obtained from the slope of $\partial(\log K_A)/\partial(\log I)$, where the sign of the slope indicates whether the ions are absorbed (positive slope) or released (negative slope).[28] The same set of experiments was performed at 10 and 55 °C to measure the effect of ion linkage on the net $\Delta H_{obs}$ within the experimental temperature range.

To determine proton linkage, the protein stock solutions were dialyzed twice in buffers with different buffer ionization enthalpies ($\Delta H_{ion}$), namely, cacodylate and ACES, at two different pH values, 6.7 and 6.1.[26] As for ion linkage, the dependence of $\Delta H_{obs}$ on $\Delta H_{ion}$, $\partial\Delta H_{obs}/\partial\Delta H_{ion}$, reports the number of protons ($n_{H^+}$) that are transferred between the proteins and the buffer, with a positive $n_{H^+}$ indicating proton uptake (protonation) and a negative $n_{H^+}$ proton release (deprotonation). With $n_{H^+}$ determined, the net binding enthalpy $\Delta H_{obs}$ was corrected, at each temperature, for the enthalpy of ionization to obtain the enthalpy of binding ($\Delta H_{bind}$):[27,29]

$$\Delta H_{obs} = \Delta H_{bind} + n_{H^+}\Delta H_{ion} \quad (6)$$

Correcting $\Delta H_{obs}$ at each temperature for the proton linkage effect yielded a corrected $\Delta C_p$ for subsequent structural−thermodynamic analysis.

**$\Delta C_p$ and Binding-Coupled Folding.** Structural−thermodynamic relationships have established empirical and theoretical links between the magnitude of $\Delta C_p$ and the extent of binding-coupled protein folding.[22,30−32] Following this approach, we used the corrected $\Delta C_p$ to obtain a thermodynamic estimate of the number of residues (**R**) that become ordered upon association of *Pfu* RPP21 and RPP29. Briefly, the approach stipulates that for a protein−protein interaction, at the $T_S$ (the temperature at which $\Delta S_{assoc}$ is zero), the entropy changes from the hydrophobic effect ($\Delta S_{HE}$) and losses of

Table 1. Temperature-Dependent Thermodynamics for Titration of RPP29 into RPP21[a]

| temp (°C) | $N$ | $K_A$ ($/10^6$) | $\Delta G$ | $\Delta H$ | $T\Delta S$ |
|---|---|---|---|---|---|
| 10 | 0.956 ± 0.063 | 9.17 ± 2.36 | −9.00 ± 0.14 | 17.10 ± 0.53 | 26.08 ± 0.4 |
| 15 | 1.015 ± 0.068 | 10.91 ± 1.98 | −9.26 ± 0.1 | 11.64 ± 0.21 | 20.90 ± 0.12 |
| 20[b] | 0.900 ± 0.014 | 9.55 ± 3.48 | −9.35 ± 0.21 | 5.95 ± 0.15 | 15.29 ± 0.26 |
| 30[b] | 0.986 ± 0.063 | 33.15 ± 4.46 | −10.42 ± 0.08 | −5.19 ± 0.45 | 5.24 ± 0.51 |
| 35 | 0.998 ± 0.101 | 20.10 ± 2.59 | −10.28 ± 0.08 | −10.25 ± 0.25 | 0.05 ± 0.27 |
| 40 | 1.030 ± 0.02 | 17.10 ± 4.17 | −10.34 ± 0.14 | −15.84 ± 1.27 | −5.49 ± 1.39 |
| 45 | 1.002 ± 0.062 | 10.66 ± 0.88 | −10.22 ± 0.05 | −23.53 ± 0.42 | −13.29 ± 0.39 |
| 55 | 0.970 ± 0.033 | 2.04 ± 0.95 | −9.40 ± 0.32 | −31.98 ± 0.51 | −22.56 ± 0.73 |

[a]The buffer consisted of 20 mM cacodylate (pH 6.7), 10 mM KCl, 0.3 mM $ZnCl_2$, and 0.02% $NaN_3$. Binding parameters are $N$ (number of RPP29 molecules binding per RPP21), $K_A$ (association equilibrium constant, in inverse molar), and $\Delta G$, $\Delta H$ and $T\Delta S$ in kilocalories per mole. Reported uncertainties are the standard deviations of the three repeat data sets at each temperature, except at 20 °C, which are standard fitting errors. Least-squares fitting of $\Delta H$ and $\Delta G$ to eqs 3 and 5 yields the following: $\Delta C_p = -1115 \pm 18$ cal mol$^{-1}$ K$^{-1}$, $T_H = 298.6 \pm 0.2$ K, and $T_S = 307.8 \pm 0.1$ K. [b]Titrations of RPP29 into RPP21 at 20 and 30 °C were performed once and twice, respectively.

rotational and translational degrees of freedom ($\Delta S_{rt}$) are balanced by other effects, including binding-induced folding ($\Delta S_{other}$).

$$\Delta S_{assoc} = 0 = \Delta S_{HE} + \Delta S_{rt} + \Delta S_{other} \quad (7)$$

$\Delta S_{HE}$ is well correlated with changes in nonpolar surface area and can be determined empirically from $\Delta C_p$ (after correction for other effects):

$$\Delta S_{HE} = 1.35\Delta C_p \ln(T_S/386) \quad (8)$$

The entropy change from the loss of rotational and translation degrees of freedom, $\Delta S_{rt}$, can be derived on statistical thermodynamic grounds to correspond to the cratic entropy of 8 cal mol$^{-1}$ K$^{-1}$,[24,33] though an empirical value of 50 ± 10 cal mol$^{-1}$ K$^{-1}$ has been found to agree with structural data;[22] we used this empirical estimate here. Finally, an empirical analysis of $\Delta S_{other}$ from folding of a number of different proteins yielded an average folding entropy cost per residue ($\Delta S_R$) of −5.6 cal mol$^{-1}$ K$^{-1}$.[22,31] Thus, $R$ was estimated from

$$R = \frac{\Delta S_{other}}{\Delta S_R} = \frac{-(\Delta S_{HE} + \Delta S_{rt})}{\Delta S_R} = \frac{1.35\Delta C_p \ln(T_S/386) - 50}{5.6} \quad (9)$$

**NMR Spectroscopy.** Two dimensional $^1H-^{15}N$ NMR spectra of [U-$^{15}$N]- and [U-$^{15}$N,$^{13}$C]RPP21 and -RPP21/A14V were recorded at 55 °C on a Bruker DRX600 instrument equipped with a cryogenically cooled triple-resonance single-axis gradient probe. Samples were at a concentration of ∼1 mM, with a slight excess of RPP29, in 10 mM Tris-HCl (pH 6.7), 10 mM KCl, 0.3 mM $ZnCl_2$, and 0.02% (w/v) $NaN_3$, and were prepared as previously described.[14,25]

## RESULTS AND DISCUSSION

**Structural−Thermodynamic Calculations.** A change in surface hydration upon formation of a macromolecular complex is generally understood to be the most significant contributor to heat capacity changes ($\Delta C_p$) that accompany binding and protein folding;[24,30,31,34] thus, in principle, this thermodynamic parameter, $\Delta C_{p,str}$, can be predicted once high-resolution structural data are available.[22,24] The interface between *Pfu* RPP21 and RPP29 in the NMR-derived structure of their 1:1 complex (Figure 1) buries 642 ± 64 Å$^2$ of polar accessible surface area ($\Delta ASA_{pol}$) and 1772 ± 79 Å$^2$ of nonpolar accessible surface area ($\Delta ASA_{np}$). Empirical structural−thermodynamic correlations (eq 1) thus predict a binding heat capacity change ($\Delta C_{p,str}$) of −630 ± 69 cal mol$^{-1}$ K$^{-1}$. This $\Delta C_{p,str}$ value is limited by the assumption of only minor changes in the interface between RPP29 and RPP21 and cannot account for contributions from changes in other linked equilibria, such as binding-coupled folding of the proteins.

**The RPP21−RPP29 Interaction Is Characterized by a Large Negative $\Delta C_p$.** Titrations of RPP29 into RPP21 performed over a temperature range from 10 to 55 °C yielded high-quality ITC data (Figure 2) that allowed accurate determination of $\Delta H_{obs}$ (enthalpy change), $K_A$ (association constant), and $N$ (stoichiometry) of binding (Figure 2, Figure S2 of the Supporting Information, and Table 1). The temperature dependence of binding enthalpy, $\partial\Delta H/\partial T$, was linear over the temperature range sampled (Figure 3); this observation permits the simplifying assumption that equilibria contributing strongly to $\Delta H$ are not substantially shifted over the temperature range sampled,[34,35] although gradual shifts in many equilibria with small contributions cannot be ruled out.[36] Fitting the enthalpy data to eq 3 yielded an experimental value for $\Delta C_{p,obs}$ of −1115 ± 18 cal mol$^{-1}$ K$^{-1}$, nearly twice that predicted from intermolecular surface burial alone (above). The data also revealed a $T_H$ of 25.4 °C (298.6 ± 0.2 K), below which the RPP21−RPP29 interaction is endothermic and above which it is exothermic (Figures 2 and 3). It is worth noting that because the enthalpy of binding is near zero at 25 °C, binding between RPP21 and RPP29 cannot be detected by ITC near this temperature, a consideration that might easily be overlooked when planning calorimetric experiments.

Despite the strong temperature dependence of $\Delta H$, the binding affinity $K_A$, and thus $\Delta G$, was relatively insensitive to temperature over the range sampled (−10.4 to −9.0 kcal/mol) (Figure 3 and Table 1). From the temperature dependence of $K_A$ and eqs 2 and 5, the temperature at which $\Delta S$ was zero, $T_S$, was 34.6 °C (307.8 ± 0.1 K). Below this temperature, binding was favored by a net entropy increase ($\Delta S > 0$) and unfavorable above ($\Delta S < 0$). The analysis also illustrates the curvature in the temperature dependence of $\Delta G$ (Figure 3).

These experiments provided access to parameters $T_S$ and $\Delta C_p$, required for structural−thermodynamic interpretation according to eq 9. However, because other linked equilibria can contribute to $\Delta C_{p,obs}$,[34,35] we sought to first identify and correct for these effects. In particular, we considered significant


dx.doi.org/10.1021/bi201674d | *Biochemistry* 2012, 51, 926−935

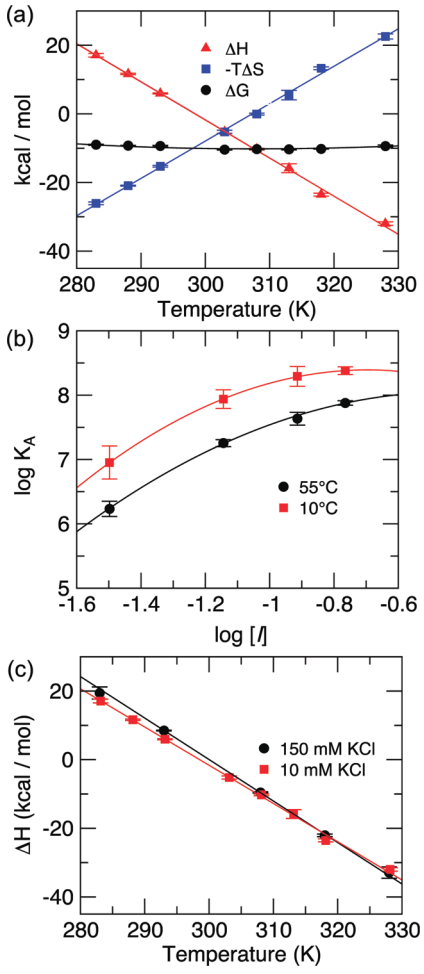


**Figure 3.** Thermodynamics of the RPP29–RPP21 interaction as measured by ITC. (a) Temperature dependence of $\Delta H$ (red triangles), $-T\Delta S$ (blue squares), and $\Delta G = -RT \ln K_A$ (black circles), obtained from fitting the calorimetric data to a one-site binding model. The line for $\Delta H$ is a linear fit of the data to eq 3, yielding a slope, $\Delta C_p$, of $-1115$ cal mol$^{-1}$ K$^{-1}$ and an $x$-intercept, $T_H$, of 298.6 K. The line for $\Delta G$ shows its curvature and represents the fit of the data to a modified Gibbs–Helmholtz relation (eq 5), which reports a $T_S$ of 307.8 K, using the $\Delta C_p$ value obtained from the slope of $\partial\Delta H/\partial T$. The line through $-T\Delta S$ was generated from eq 4 using the best-fit values from $\partial\Delta H/\partial T$ and $\partial\Delta G/\partial T$. Uncertainty in plotted thermodynamic values represents the standard deviation of three measurements repeated under the same conditions, except for 20 °C (single) and 30 °C (duplicate). (b) Ion linkage as assessed by the effect of ionic strength on the calorimetrically determined $K_A$. Lines represent phenomenological fits of the data to a quadratic of the form $ax^2 + bx + c$. The slopes of the log $K_A$ vs log $I$ relationship at 55 °C (black) and 10 °C (red) are positive at a low ionic strength (~3.5 at 30 mM), indicating ion uptake upon binding; negative slopes are implied at higher $I$ values but could not be measured because of precipitation of the sample at higher salt concentrations. (c) Temperature dependence of $\Delta H$ at two different KCl concentrations, 10 and 150 mM. Best-fit values at 150 mM KCl are within error of those at 10 mM KCl.

contributions to $\Delta C_{p,obs}$ from ion and proton linkage, and burial of interfacial water molecules, which have been described as significant contributors to $\Delta C_{p,obs}$ in other systems.[28,29,36−41]

**RPP21–RPP29 Binding Is Accompanied by Ion Uptake with a Small Effect on $\Delta C_p$.** Two intermolecular ion pairs have been observed in the RPP21–RPP29 interface from both *Pfu* and *Pho*.[14,42] Glu47 and Asp72 of *Pfu* RPP29 are observed to pair with Arg17 and Arg38 of *Pfu* RPP21,[14] and a similar interface is observed in the *Pho* RPP21–RPP29 complex.[42] On the basis of this observation, it was reasonable to expect an effect on the RPP21–RPP29 interaction from changes in solution ionic strength because favorable electrostatic contacts would be weakened at high salt concentrations.[43,44] Despite this expectation, the binding affinity $K_A$ increased with an increasing ionic strength, $I$ (Figure 3 and Figure S3 and Table S1 of the Supporting Information). The $\partial(\log K_A)/\partial(\log I)$ trend appeared to be nonlinear over the ionic strengths sampled. Although exploring in depth the underpinnings for this nonlinear ionic strength dependence is beyond the scope of this study, similar behavior has been reported phenomenologically before,[37] and we surmise it reflects equilibria between binding-incompetent conformations at lower ionic strengths and competition between protein–protein and protein–solute ion pairing interactions at higher ionic strengths.

At 55 °C and an $I$ of 30 mM (i.e., the conditions of the NMR experiments[14]), the slope of $\partial(\log K_A)/\partial(\log I)$ was 3.5, indicating that uptake of this many ions, not release, is linked to RPP21–RPP29 binding (Figure 3).[28] At 10 °C, a similar ionic strength dependence is observed, with a slope of 3.7 at an $I$ of 30 mM. Notably, the nonlinear dependence of $\partial(\log K_A)/\partial(\log I)$ implies that at higher ionic strengths, ion release favors protein binding, as predicted from the structurally observed intermolecular ion pair. The nonintegral number of absorbed ions may be understood by considering the relatively nonspecific interaction between solvent ions and an ensemble of unfolded states for the proteins, in which the screening ions transiently exchange between protein and solvent.[45] Unfortunately, precipitation of the sample at higher ionic strengths prevented sampling a wider range of ionic conditions, and a more complete characterization of the effect.

These experiments established thermodynamic linkage between ions and protein binding. The contribution of this linkage effect to $\Delta C_{p,obs}$ was directly assessed from independent measurements of $\partial\Delta H_{obs}/\partial T$ at the ionic strengths of interest. Titrations of RPP21 into RPP29 performed in 150 mM KCl over a temperature range from 10 to 55 °C revealed a slightly larger $\Delta C_p$ of $-1177 \pm 15$ cal mol$^{-1}$ K$^{-1}$, almost within experimental error of those in 10 mM KCl (Figure 3). Thus, while ion linkage is observed to significantly affect the affinity of the RPP21–RPP29 interaction, we find that over the range of 10–150 mM KCl, it does not contribute significantly to $\Delta C_{p,obs}$.

**RPP21–RPP29 Binding Involves Net Proton Release.** To assess proton linkage in the RPP21–RPP29 interaction, $\Delta H_{obs}$ values were measured from ITC titrations at pH 6.7 in buffers with highly divergent ionization enthalpies: cacodylate ($\Delta H_{ion} = -1.334$ kcal/mol at 55 °C) and ACES ($\Delta H_{ion} = 6.922$ kcal/mol at 55 °C) (Table 2 and Figure S4 of the Supporting Information).[26] These experiments revealed a $\partial\Delta H_{obs}/\partial\Delta H_{ion}$ of $-0.7$, indicating release of protons by the proteins to the bulk solvent as a result of complex formation (Table 2).[27,29] Considering the noninteger proton linkage number and the fact that the p$K_a$ of the imidazole group of histidine side chains (which might be involved in coupled folding) is typically between pH 5 and 8,[46,47] we postulated that lowering the pH should increase the linkage number. To test this premise, we performed analogous ITC experiments in cacodylate and ACES buffers at pH 6.1, which yielded a new linkage number of $-1.1$. These experiments demonstrate that the binding of RPP21 to RPP29 is accompanied by net deprotonation and most likely

**Table 2. Proton Linkage Revealed by the Thermodynamics of Titration of RPP29 into RPP21 in Buffers with Different Ionization Enthalpies ($\Delta H_{ion}$) at pH 6.1 and 6.7 and at 55 °C[a]**

| pH | buffer | $\Delta H_{ion}$[b] (kcal/mol) | $\Delta H_{obs}$ (kcal/mol) | $\partial\Delta H_{obs}/\partial\Delta H_{ion}$ |
|---|---|---|---|---|
| 6.7 | cacodylate | −1.334 | −32.0 ± 0.5 | −0.7 |
| | ACES | 6.922 | −37.6 ± 0.4 | |
| 6.1 | cacodylate | −1.344 | −34.3 ± 0.1 | −1.1 |
| | ACES | 6.922 | −43.0 ± 0.2 | |

[a]Reported values are the average and standard deviation of three replicates at pH 6.7, and average and root-mean-square deviation of the error of two replicates at pH 6.1. [b]The buffer ionization enthalpies at 55 °C are from published values of $\Delta H_{ion}$ and $\Delta C_p$ at 25 °C.[26]

implicate histidine side chains. Note that the experimentally observed linkage numbers could correspond to ionization at one site, or at multiple sites with similar p$K_a$ values.

We sought a structural explanation for the observed proton linkage. There are six histidine residues in the *Pfu* RPP21−RPP29 complex. Four of them (His60$^{RPP29}$, His67$^{RPP21}$, His87$^{RPP21}$, and His97$^{RPP21}$) are distal from the protein−protein interface and are in well-structured regions of the free proteins.[14] However, two histidines in RPP29 are in the dimer interface, His34$^{RPP29}$ and His46$^{RPP29}$ (Figure 4); the

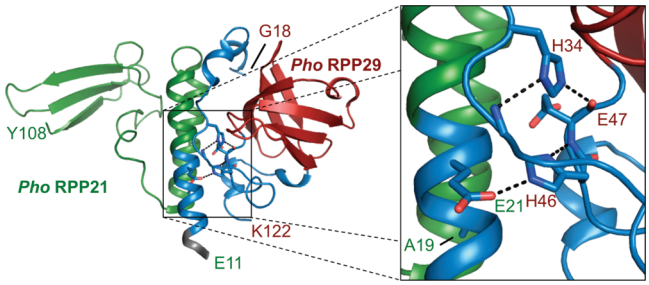


**Figure 4.** Hydrogen bonds to histidine side chains in the crystal structure of the *Pho* RPP21−RPP29 complex (PDB entry 2ZAE) provide a structural explanation for proton linkage in the binding of *Pfu* RPP21 and RPP29. The left panel shows a cartoon diagram of the *Pho* RPP21−RPP29 complex colored as in Figure 1. The boxed region in the left panel is magnified at the right, showing the four possible hydrogen bonds. Three of them are intramolecular hydrogen bonds in RPP29 between acceptor E47O and protonated donor H34 N$\varepsilon$2, donor G36N and deprotonated acceptor H34 N$\delta$1, and deprotonated acceptor H46 N$\delta$1 and donor E47N within RPP29. One intermolecular hydrogen bond was also observed between acceptor RPP21 E21 O$\varepsilon$2 and protonated donor RPP29 H46 N$\varepsilon$2. The residue numbers are labeled in green for RPP21 and red for RPP29.

latter, albeit not universally present, is highly conserved among archaeal RPP29 homologues.[14] Moreover, both are in the region of the protein (residues 17−48) that is believed to fold upon binding, based on the absence of backbone resonances from NMR spectra in the absence of RPP21.[14] Without knowledge of the protonation states of histidine side chains, all histidines were assumed to be protonated at both N$\varepsilon$2 and N$\delta$1 positions during computational refinement of the solution structure of the *Pfu* RPP21−RPP29 complex.[14] Consequently, structure calculations could not yield structures in which a deprotonated imidazole nitrogen could accept a hydrogen bond. However, in the homologous *Pho* RPP21−RPP29 crystal structure,[42] these histidines in RPP29 appear to be involved in hydrogen bonding interactions that can be accommodated only by N$\delta$1-deprotonated, N$\varepsilon$2-protonated imidazole rings, both donating and accepting hydrogen bonds; three of those hydrogen bonds are intramolecular, and one is to a glutamate (Glu21$^{RPP21}$) side chain carboxylate in RPP21 that is also conserved between *Pfu* and *Pho* (Figure 4 and Figure S6 of the Supporting Information). Thus, deprotonation-dependent hydrogen bonding interactions by one or both of these histidine side chains are a likely source of the experimentally determined proton linkage.

Having identified proton linkage as a contributor to $\Delta C_{p,obs}$, we proceeded to correct this value using eqs 3 and 6.[27,29] Because the ITC experiments were conducted in cacodylate buffer, which has a low $\Delta H_{ion}$ (−0.717 kcal/mol at 25 °C) (Table 2) and a weak temperature dependence (−20.55 cal mol$^{-1}$ K$^{-1}$),[26] linkage of a single proton required minimal correction of $\Delta C_p$ to −1100 ± 18 cal mol$^{-1}$ K$^{-1}$. This analysis leaves an excess $\Delta C_p$ of ∼500 cal mol$^{-1}$ K$^{-1}$ ($\Delta C_{p,obs} - \Delta C_{p,str}$) for which ion and proton binding cannot account.

**Burial of Structured Water.** The burial of water molecules in a molecular interface has been argued on experimental and theoretical grounds to be a significant source of $\Delta C_{p,obs}$ in interactions involving proteins.[36,39−41] Literature estimates of the contribution to $\Delta C_p$ from burying a water molecule (i.e., being transferred from the solvent to the protein) vary widely, from nearly negligible to that of the heat capacity of water (18 cal mol$^{-1}$ K$^{-1}$)[48] to as much as 72 cal mol$^{-1}$ K$^{-1}$ for a completely buried water molecule making four hydrogen bonds.[36] On the basis of these approximations, for the excess $\Delta C_p$ of ∼500 kcal mol$^{-1}$ K$^{-1}$ to be contributed by binding water, on the order of 7−28 water molecules would have to be fully sequestered upon formation of the RPP21−RPP29 complex.

To indirectly assess whether significant numbers of water molecules might become sequestered in the interface upon binding, we examined ordered water molecules in the 2.2 Å crystal structure of the highly homologous *Pho* RPP21−RPP29 complex (PDB entry 2ZAE) (Figure S6 of the Supporting Information).[42] In this structure, there are two copies of the RPP21−RPP29 complex in the asymmetric unit, providing additional confidence in the identification of structured waters. Well-defined density within a cavity inside RPP29 has been assigned to a water molecule modeled within hydrogen bonding distance of the carboxylate side chains of Glu47 and Glu73, and the backbone amides of Leu48 and Ile49. Though not in direct intramolecular contact with other residues, Glu47$^{RPP29}$ is positioned to form an intermolecular ion pair with the guanidinium group of Arg17$^{RPP21}$ [Arg22 in *Pho* (Figure S6 of the Supporting Information)]. Moreover, Glu47$^{RPP29}$ and Leu48$^{RPP29}$ are in a poorly structured region in the free *Pfu* protein. Consequently, if coupled folding of RPP29 involves sequestration of the crystallographically observed water molecule, this too could contribute to $\Delta C_{p,obs}$. Although this premise is difficult to confirm experimentally,[39] if we assume that four new hydrogen bonds are formed upon binding-coupled folding, this could contribute as much as 72 cal mol$^{-1}$ K$^{-1}$ to $\Delta C_{p,obs}$.[36] Additional ordered water molecules were observed in the *Pho* RPP21−RPP29 complex, 23 of which are within 1 Å of an asymmetry-related water molecule. However, these are either mostly surface-exposed or far from the protein−protein interface and therefore would not be expected to contribute significantly to binding $\Delta C_{p,obs}$, unless their ordering accompanies the binding-coupled folding of


dx.doi.org/10.1021/bi201674d | *Biochemistry* 2012, 51, 926−935

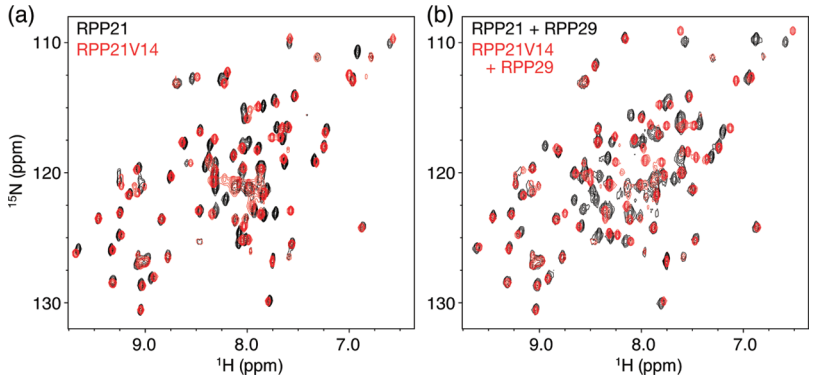


**Figure 5.** Two-dimensional $^{1}$H−$^{15}$N NMR spectra of RPP21 and RPP21/A14V free and bound to RPP29 reveal differing extents of coupled folding. Overlay of portions of the correlation spectra of RPP21 (black) and RPP21/A14V (red) in their free states (a) and in the presence of RPP29 (b).

those regions of the protein with which they interact. Because such changes in protein solvation would be included in the empirically determined parameter $\Delta S_R$,[22] we do consider them explicitly here. If only a single buried interfacial water molecule is taken as a contributor to $\Delta C_{p,obs}$, this value can be corrected from −1100 to −1028 cal mol$^{-1}$ K$^{-1}$.

**The Extent of Coupled Folding from ITC Agrees with NMR Data.** Application of eq 9 to the experimentally determined $T_S$ (308 K) and corrected $\Delta C_p$ (−1028 cal mol$^{-1}$ K$^{-1}$) of the *Pfu* RPP21−RPP29 interaction yields an ***R*** of 47, providing a numerical estimate for the effective number of residues that fold upon binding. This number agrees favorably with the NMR-observed folding of 50 residues upon formation of the *Pfu* RPP21−RPP29 complex, despite the different metrics involved in the two techniques (Figure 1; residues 17−48 and 116−123 of RPP29 and residues 9−18 of RPP21).[14] In the NMR studies, "foldedness" was assessed on the basis of the observation and assignment of resonances in standard triple-resonance NMR experiments. Because residues in regions of the protein that are metastable are subject to conformational sampling on time scales that lead to loss of NMR signals,[49] the absence of signals from such regions is often interpreted as indicative of poorly formed structure. Population of such alternative conformations directly leads to an increase in $C_p$, compared to a protein with a single stable conformation,[30,34,35] but also through the reorganization of solvent molecules and ions that facilitate folding. Thus, in the case of binding-coupled folding, the large excess negative $\Delta C_p$ arises from narrowing of the energy landscape through reduction in the number of conformations that can be significantly populated by the protein and its tightly associated ligands (including ions and water molecules).

This explanation for the magnitude of $\Delta C_p$ was corroborated by NMR and ITC studies of a point mutant that interferes with proper formation of the RPP21−RPP29 interface. NMR studies of the interaction between RPP29 and a variant of RPP21 with an Ala to Val substitution at position 14 (RPP21/A14V) revealed a similar extent of binding-coupled protein folding in RPP29, but not in RPP21/A14V. That is, 40 residues from RPP29 (17−48 and 116−123) that did not produce NMR signals in the free protein were observed in the accompanying complex with RPP21/A14V. However, residues 9−18 that give rise to observable signals in the wild-type complex (Figure 1) cannot be assigned in the complex of RPP21/A14V with RPP29.[14,17,25] Moreover, because Ala14 is in the region of RPP21 that is unstructured in the absence of RPP29 (Figure 1) but makes important intermolecular packing interactions in the complex, this mutation can be expected to affect RPP29 binding more than the integrity of the RPP21 structure. Indeed, $^{1}$H−$^{15}$N NMR spectra of RPP21 and RPP21/A14V are more similar than the corresponding spectra of their complexes with RPP29 (Figure 5); nevertheless, the differences in the spectra of the free proteins do indicate that in the free protein Val14 does measurably perturb the RPP21 structure, indicating that this region of the free protein is not fully unfolded. We determined $\Delta C_p$ for this interaction via ITC, by measuring $\Delta H_{obs}$ of binding from 5 to 55 °C, yielding a $\Delta C_{p,obs}$ of −932 cal mol$^{-1}$ K$^{-1}$. This value was corrected by assuming, as for the wild-type interaction, (1) an insignificant contribution from ion binding to $\Delta C_p$, (2) 0.7 proton transfer upon binding at pH 6.7, and (3) sequestration of one water molecule at a cost of 72 cal mol$^{-1}$ K$^{-1}$. This yielded a $\Delta C_p$ of −845 cal mol$^{-1}$ K$^{-1}$ and a $T_S$ of 304 K for the wild-type *Pfu* RPP29−RPP21/A14V interaction (Figure 6 and Figure S5 and Table S3 of the Supporting Information). Application of eq 9 to these values estimates an ***R*** of 40 residues folding upon binding. This result is qualitatively consistent with the reduced extent of binding-coupled protein folding evident from the NMR spectra for the interaction of the RPP21/A14V point mutant with RPP29 (40 for the mutant and 50 for the wild type).

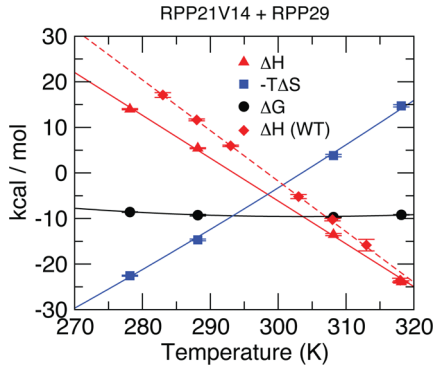


**Figure 6.** Temperature dependence of thermodynamic parameters for the interaction of *Pfu* RPP21/A14V with RPP29. Legend like that of Figure 3a; the $\Delta H$ for the wild-type (WT) proteins is also included for comparison (red diamonds, dashed line). A $\Delta C_p$ (−932 cal mol$^{-1}$ K$^{-1}$) was obtained by fitting the $\Delta H$ data to eq 3, and $T_S$ (304 K), from eq 5. The smaller negative $\Delta C_p$ (i.e., less steep slope) is consistent with less coupled folding for the mutant than for the wild type.


dx.doi.org/10.1021/bi201674d | *Biochemistry* 2012, 51, 926−935

**Caveats and Sources of Uncertainty.** Structural interpretation of thermodynamic data[22,24] is complicated by the many interactions that contribute to the net thermodynamic parameters measured, and imprecise knowledge of the magnitude of the effects. As noted above, changes in protein solvation are generally considered to be the major contributor to a negative $\Delta C_p$ of binding, via the hydrophobic effect,[30,31,34,50] though estimates of the empirical relation between surface area burial and $\Delta C_p$ differ.[24,50] Moreover, binding-induced heat capacity changes in excess of $\Delta C_{p,\mathrm{str}}$ are common in protein−ligand, protein−DNA, and protein−protein interactions, even in systems with little evidence of coupled conformational changes,[32,39,51] complicating efforts to obtain insightful structural−thermodynamic correlations. Similarly, the contribution to $\Delta C_p$ from the complete or partial burial of water molecules upon formation of a protein−protein complex is difficult to estimate accurately, and it seems likely that its magnitude will be highly system-dependent. Lastly, estimates of $R$, the number of residues that fold upon binding, are further dependent on $\Delta S_R$, an empirical estimate of the per-residue entropy change that accompanies folding;[22,31] though not explicitly considered in the development of that parameter, it seems likely that $\Delta S_R$ includes contributions from multiple coupled equilibria, including coupled binding of water molecules, ions, and changes in ionization.

Thus, the quantitative insights from these studies are tempered by a number of sources of uncertainty, if of unequal scope and magnitude: (1) the accuracy in obtaining the relevant calorimetric data ($\Delta H_{\mathrm{obs}}$, $\Delta C_p$, $T_S$, and $K_A$), (2) the imperfect empirical relationships between $\Delta C_p$ and $\Delta S_{\mathrm{HE}}$ and in the estimation of $\Delta S_R$, (3) the magnitude of the effect of binding-coupled water sequestration on $\Delta C_{p,\mathrm{obs}}$, and (4) the imperfect correlation between the NMR spectroscopic metric of foldedness and the thermodynamic parameters measured. Despite these limitations, by integrating complementary spectroscopic, crystallographic, and mutagenesis data, we are able to provide significant qualitative, if not highly quantitative, structural−thermodynamic insights into the interaction between these protein components of archaeal RNase P.

## CONCLUSION

We have used ITC to gain insights into the disorder to structure transition that accompanies formation of the heterodimer comprising *Pfu* RPP21 and RPP29, two subunits of archaeal RNase P. Titrations uncovered a large negative excess $\Delta C_p$ that could not be ascribed to ion or proton linkage, or sequestration of interfacial water molecules, thereby establishing strong thermodynamic linkage of protein folding to binding; the magnitude of this effect is consistent with that expected from qualitative NMR studies. Ion linkage experiments revealed unexpected ion uptake at low ionic strengths, suggesting that electrostatic repulsion disfavors formation of favorable intra- and intermolecular interactions that otherwise stabilize the complex, while proton linkage measurements suggest that histidine side chain deprotonation is required for proper folding and binding. These data provide both global and site-specific insights into the structural and thermodynamic basis for the specific interaction between these highly charged and thermostable proteins, which subsequently assemble with a large RNase P RNA subunit to facilitate tRNA 5′ maturation.

The binding-coupled folding of *Pfu* RPP21 and RPP29 exemplifies the notion that intermolecular interactions are required for formation of functionally relevant structures. Such induced fit, and its implied conformational sampling, lowers the energy barrier for generating complementary macromolecular interfaces and acts as a gating mechanism that allows biological function only upon completion of an array of conformational switches.[22,52−55] Indeed, the unique structural features resulting from coupled folding during assembly of the *Pfu* RPP21−RPP29 complex are likely critical for generating its high-affinity, RNA-binding surface. Although the dramatic changes observed during formation of the *Pfu* RPP21−RPP29 heterodimer are not mirrored in the *Pfu* POP5−RPPP30 complex,[56,57] we recently demonstrated induced fit during assembly of the archaeal RNase P holoenzyme, wherein the *Pfu* RNase P RNA could rescue in vitro a 24-amino acid deletion in RPP29 that compromised its ability to bind RPP21.[58] Therefore, it appears that cofolding of interacting pairs in large RNPs represents a general theme for achieving the specificity and functional payoffs from induced-fit mechanisms.

## ASSOCIATED CONTENT

### Supporting Information

Tables of thermodynamic data, sequence alignments, and representative calorimetric thermograms. This material is available free of charge via the Internet at http://pubs.acs.org.

## AUTHOR INFORMATION


### Corresponding Author

*Address: 484 W. 12th Ave., Columbus, OH 43210. Phone: (614) 292-1377. Fax: (614) 292-6773. E-mail: foster.281@osu.edu.

### Present Address

∥Genentech Inc., 1 DNA Way, MS 97B, South San Francisco, CA 94080. Phone: (650) 467-6613. E-mail: yirenxujoy@gmail.com.



### Funding

This work was supported by a grant from the National Institutes of Health (NIH) to M.P.F. and V.G. (GM067807) and a grant from the National Science Foundation to V.G. (MCB 0843543); funds for the ITC200 microcalorimeter were provided by an NIH ARRA supplement to R01 GM063615 to T. M. Henkin and M.P.F.

## ACKNOWLEDGMENTS

We thank I. R. Kleckner and E. Ihms for helpful discussions.


## ABBREVIATIONS

RNase P, ribonuclease P; RNP, ribonucleoprotein; RPR, RNase P RNA; RPP, RNase P protein; *Pfu*, *P. furiosus*; *Pho*, *P. horikoshii*; ASA, accessible surface area.

## REFERENCES


(1) Altman, S. (2007) A view of RNase P. *Mol. BioSyst. 3*, 604−607.

(2) Jarrous, N., and Gopalan, V. (2010) Archaeal/Eukaryal RNase P: subunits, functions and RNA diversification. *Nucleic Acids Res. 38*, 7885−7894.

(3) Evans, D, Marquez, S. M., and Pace, N. R. (2006) RNase P: Interface of the RNA and protein worlds. *Trends Biochem. Sci. 31*, 333−341.

(4) Guerrier-Takada, C., Gardiner, K., Marsh, T., Pace, N., and Altman, S. (1983) The RNA moiety of ribonuclease P is the catalytic subunit of the enzyme. *Cell 35*, 849−857.

(5) Chamberlain, J. R., Lee, Y., Lane, W. S., and Engelke, D. R. (1998) Purification and characterization of the nuclear RNase P

holoenzyme complex reveals extensive subunit overlap with RNase MRP. *Genes Dev. 12*, 1678−1690.
(6) Kikovska, E., Svard, S. G., and Kirsebom, L. A. (2007) Eukaryotic RNase P RNA mediates cleavage in the absence of protein. *Proc. Natl. Acad. Sci. U.S.A. 104*, 2062−2067.
(7) Pannucci, J. A., Haas, E. S., Hall, T. A., Harris, J. K., and Brown, J. W. (1999) RNase P RNAs from some Archaea are catalytically active. *Proc. Natl. Acad. Sci. U.S.A. 96*, 7803−7808.
(8) Gopalan, V. (2007) Uniformity amid diversity in RNase P. *Proc. Natl. Acad. Sci. U.S.A. 104*, 2031−2032.
(9) Hartmann, E., and Hartmann, R. K. (2003) The enigma of ribonuclease P evolution. *Trends Genet. 19*, 561−569.
(10) Hall, T. A., and Brown, J. W. (2002) Archaeal RNase P has multiple protein subunits homologous to eukaryotic nuclear RNase P proteins. *RNA 8*, 296−306.
(11) Tsai, H. Y., Pulukkunat, D. K., Woznick, W. K., and Gopalan, V. (2006) Functional reconstitution and characterization of *Pyrococcus furiosus* RNase P. *Proc. Natl. Acad. Sci. U.S.A. 103*, 16147−16152.
(12) Chen, W. Y., Pulukkunat, D. K., Cho, I. M., Tsai, H. Y., and Gopalan, V. (2010) Dissecting functional cooperation among protein subunits in archaeal RNase P, a catalytic ribonucleoprotein complex. *Nucleic Acids Res. 38*, 8316−8327.
(13) Pulukkunat, D. K., and Gopalan, V. (2008) Studies on *Methanocaldococcus jannaschii* RNase P reveal insights into the roles of RNA and protein cofactors in RNase P catalysis. *Nucleic Acids Res. 36*, 4172−4180.
(14) Xu, Y., Amero, C. D., Pulukkunat, D. K., Gopalan, V., and Foster, M. P. (2009) Solution structure of an archaeal RNase P binary protein complex: Formation of the 30-kDa complex between *Pyrococcus furiosus* RPP21 and RPP29 is accompanied by coupled protein folding and highlights critical features for protein-protein and protein-RNA interactions. *J. Mol. Biol. 393*, 1043−1055.
(15) Cho, I. M., Lai, L. B., Susanti, D., Mukhopadhyay, B., and Gopalan, V. (2010) Ribosomal protein L7Ae is a subunit of archaeal RNase P. *Proc. Natl. Acad. Sci. U.S.A. 107*, 14573−14578.
(16) Fukuhara, H., Kifusa, M., Watanabe, M., Terada, A., Honda, T., Numata, T., Kakuta, Y., and Kimura, M. (2006) A fifth protein subunit Ph1496p elevates the optimum temperature for the ribonuclease P activity from *Pyrococcus horikoshii* OT3. *Biochem. Biophys. Res. Commun. 343*, 956−964.
(17) Amero, C. D., Boomershine, W. P., Xu, Y., and Foster, M. (2008) Solution structure of *Pyrococcus furiosus* RPP21, a component of the archaeal RNase P holoenzyme, and interactions with its RPP29 protein partner. *Biochemistry 47*, 11704−11710.
(18) Kakuta, Y., Ishimatsu, I., Numata, T., Kimura, K., Yao, M., Tanaka, I., and Kimura, M. (2005) Crystal structure of a ribonuclease P protein Ph1601p from *Pyrococcus horikoshii* OT3: An archaeal homologue of human nuclear ribonuclease P protein Rpp21. *Biochemistry 44*, 12086−12093.
(19) Boomershine, W. P., McElroy, C. A., Tsai, H. Y., Wilson, R. C., Gopalan, V., and Foster, M. P. (2003) Structure of Mth11/Mth Rpp29, an essential protein subunit of archaeal and eukaryotic RNase P. *Proc. Natl. Acad. Sci. U.S.A. 100*, 15398−15403.
(20) Numata, T., Ishimatsu, I., Kakuta, Y., Tanaka, I., and Kimura, M. (2004) Crystal structure of archaeal ribonuclease P protein Ph1771p from *Pyrococcus horikoshii* OT3: An archaeal homolog of eukaryotic ribonuclease P protein Rpp29. *RNA 10*, 1423−1432.
(21) Sidote, D. J., Heideker, J., and Hoffman, D. W. (2004) Crystal structure of archaeal ribonuclease P protein aRpp29 from *Archaeoglobus fulgidus*. *Biochemistry 43*, 14128−14138.
(22) Spolar, R. S., and Record, M. T. Jr. (1994) Coupling of local folding to site-specific binding of proteins to DNA. *Science 263*, 777−784.
(23) Willard, L., Ranjan, A., Zhang, H., Monzavi, H., Boyko, R. F., Sykes, B. D., and Wishart, D. S. (2003) VADAR: A web server for quantitative evaluation of protein structure quality. *Nucleic Acids Res. 31*, 3316−3319.
(24) Lavigne, P., Bagu, J. R., Boyko, R., Willard, L., Holmes, C. F., and Sykes, B. D. (2000) Structure-based thermodynamic analysis of the dissociation of protein phosphatase-1 catalytic subunit and microcystin-LR docked complexes. *Protein Sci. 9*, 252−264.
(25) Xu, Y. (2010) Structure and interactions of archaeal RNase P proteins RPP29 and RPP21. Ph.D. Thesis, Department of Biochemistry, The Ohio State University, Columbus, OH, p 254.
(26) Goldberg, R. Y., et al. (2002) Thermodynamic Quantities for the Ionization Reactions of Buffers. *J. Phys. Chem. Ref. Data 31*, 231−370.
(27) Jelesarov, I., and Bosshard, H. R. (1999) Isothermal titration calorimetry and differential scanning calorimetry as complementary tools to investigate the energetics of biomolecular recognition. *J. Mol. Recognit. 12*, 3−18.
(28) Lohman, T. M., Overman, L. B., Ferrari, M. E., and Kozlov, A. G. (1996) A highly salt-dependent enthalpy change for *Escherichia coli* SSB protein-nucleic acid binding due to ion-protein interactions. *Biochemistry 35*, 5272−5279.
(29) Baker, B. M., and Murphy, K. P. (1996) Evaluation of linked protonation effects in protein binding reactions using isothermal titration calorimetry. *Biophys. J. 71*, 2049−2055.
(30) Sturtevant, J. M. (1977) Heat capacity and entropy changes in processes involving proteins. *Proc. Natl. Acad. Sci. U.S.A. 74*, 2236−2240.
(31) Baldwin, R. L. (1986) Temperature dependence of the hydrophobic interaction in protein folding. *Proc. Natl. Acad. Sci. U.S.A. 83*, 8069−8072.
(32) Spolar, R. S., Livingstone, J. R., and Record, M. T. Jr. (1992) Use of liquid hydrocarbon and amide transfer data to estimate contributions to thermodynamic functions of protein folding from the removal of nonpolar and polar surface from water. *Biochemistry 31*, 3947−3955.
(33) Kauzmann, W. (1959) Some factors in the interpretation of protein denaturation. *Adv. Protein Chem. 14*, 1−63.
(34) Prabhu, N. V., and Sharp, K. A. (2005) Heat capacity in proteins. *Annu. Rev. Phys. Chem. 56*, 521−548.
(35) Eftink, M. R., Anusiem, A. C., and Biltonen, R. L. (1983) Enthalpy-entropy compensation and heat capacity changes for protein-ligand interactions: General thermodynamic models and data for the binding of nucleotides to ribonuclease A. *Biochemistry 22*, 3884−3896.
(36) Cooper, A. (2005) Heat capacity effects in protein folding and ligand binding: A re-evaluation of the role of water in biomolecular thermodynamics. *Biophys. Chem. 115*, 89−97.
(37) Kozlov, A. G., and Lohman, T. M. (1998) Calorimetric studies of *E. coli* SSB protein-single-stranded DNA interactions. Effects of monovalent salts on binding enthalpy. *J. Mol. Biol. 278*, 999−1014.
(38) Kozlov, A. G., and Lohman, T. M. (2000) Large contributions of coupled protonation equilibria to the observed enthalpy and heat capacity changes for ssDNA binding to *Escherichia coli* SSB protein. *Proteins* No. Suppl. 4, 8−22.
(39) Bergqvist, S., Williams, M. A., O'Brien, R., and Ladbury, J. E. (2004) Heat capacity effects of water molecules and ions at a protein-DNA interface. *J. Mol. Biol. 336*, 829−842.
(40) Morton, C. J., and Ladbury, J. E. (1996) Water-mediated protein-DNA interactions: The relationship of thermodynamics to structural detail. *Protein Sci. 5*, 2115−2118.
(41) Ladbury, J. E., Wright, J. G., Sturtevant, J. M., and Sigler, P. B. (1994) A thermodynamic study of the trp repressor-operator interaction. *J. Mol. Biol. 238*, 669−681.
(42) Honda, T., Kakuta, Y., Kimura, K., Saho, J., and Kimura, M. (2008) Structure of an archaeal homolog of the human protein complex Rpp21-Rpp29 that is a key core component for the assembly of active ribonuclease P. *J. Mol. Biol. 384*, 652−662.
(43) Record, M. T. Jr., Lohman, M. L., and De Haseth, P. (1976) Ion effects on ligand-nucleic acid interactions. *J. Mol. Biol. 107*, 145−158.
(44) Record, M. T. Jr., Anderson, C. F., and Lohman, T. M. (1978) Thermodynamic analysis of ion effects on the binding and conformational equilibria of proteins and nucleic acids: The roles of ion association or release, screening, and ion effects on water activity. *Q. Rev. Biophys. 11*, 103−178.

(45) Bergqvist, S., Williams, M. A., O'Brien, R., and Ladbury, J. E. (2002) Reversal of halophilicity in a protein-DNA interaction by limited mutation strategy. *Structure 10*, 629−637.
(46) Markley, J. L., and Finkenstadt, W. R. (1975) Correlation proton magnetic resonance studies at 250 MHz of bovine pancreatic ribonuclease. III. Mutual electrostatic interaction between histidine residues 12 and 119. *Biochemistry 14*, 3562−3566.
(47) Edgcomb, S. P., and Murphy, K. P. (2002) Variability in the pKa of histidine side-chains correlates with burial within proteins. *Proteins 49*, 1−6.
(48) Dunitz, J. (1994) The Entropic Cost of Bound Water in Crystals and Biomolecules. *Science 264*, 670.
(49) Kleckner, I. R., and Foster, M. P. (2011) An introduction to NMR-based approaches for measuring protein dynamics. *Biochim. Biophys. Acta 1814*, 942−968.
(50) Murphy, K. P., Privalov, P. L., and Gill, S. J. (1990) Common features of protein unfolding and dissolution of hydrophobic compounds. *Science 247*, 559−561.
(51) Olsson, T. S., Ladbury, J. E., Pitt, W. R., and Williams, M. A. (2011) Extent of enthalpy-entropy compensation in protein-ligand interactions. *Protein Sci. 20*, 1607−1618.
(52) Leulliot, N., and Varani, G. (2001) Current topics in RNA-protein recognition: Control of specificity and biological function through induced fit and conformational capture. *Biochemistry 40*, 7947−7956.
(53) Williamson, J. R. (2000) Induced fit in RNA-protein recognition. *Nat. Struct. Biol. 7*, 834−837.
(54) Schroeder, R., Barta, A., and Semrad, K. (2004) Strategies for RNA folding and assembly. *Nat. Rev. Mol. Cell Biol. 5*, 908−919.
(55) Williamson, J. R. (2008) Cooperativity in macromolecular assembly. *Nat. Chem. Biol. 4*, 458−465.
(56) Kawano, S., Nakashima, T., Kakuta, Y., Tanaka, I., and Kimura, M. (2006) Crystal structure of protein Ph1481p in complex with protein Ph1877p of archaeal RNase P from *Pyrococcus horikoshii* OT3: Implication of dimer formation of the holoenzyme. *J. Mol. Biol. 357*, 583−591.
(57) Crowe, B. L., Bohlen, C. J., Wilson, R. C., Gopalan, V., and Foster, M. P. (2011) Assembly of the Complex between Archaeal RNase P Proteins RPP30 and Pop5. *Archaea*, doi: 10.1155/2011/891531.
(58) Chen, W. Y., Xu, Y., Cho, I. M., Oruganti, S. V., Foster, M. P., and Gopalan, V. (2011) Cooperative RNP Assembly: Complementary Rescue of Structural Defects by Protein and RNA Subunits of Archaeal RNase P. *J. Mol. Biol. 411*, 368−383.